Chapter 3

Residual Stress Analysis of Laser Remanufacturing

Shi-yun Dong, Chao-qun Song, Xiang-yi Feng,
Yong-jian Li and Shi-xing Yan

Additional information is available at the end of the chapter

http://dx.doi.org/10.5772/intechopen.72749

Abstract

Laser remanufacturing is an advanced repairing method to remanufacture damaged parts based on laser processing, such as laser cladding and laser welding. As a critical factor in determining the remanufacturing quality, residual stress of different laser-remanufactured parts was analysed by numerical methods based on deactivating and reactivating element theory, as well as experimental methods such as X-ray diffraction and hole drilling measurements. The distributions and evolution law of residual stress during multipass laser welding of 7A52 high-strength aluminium alloy, and the effects of forming strategy, heat input and solid-state phase transition on residual stress in the laser cladding forming layers of QT 500 cast iron and FV520B high strength steel, were emphatically studied. The simulation results of residual stress fit well with the experimental results, indicating that both residual stress and its accumulation phenomenon would occur during the laser welding and laser cladding forming, and were affected by factors such as welding pass, heat input and phase transition. It is feasible to control residual stress by using cross path forming strategy, less heat input and alloying power materials with low martensite transition point (Ms).

Keywords: residual stress, phase transition, laser remanufacturing, finite element analysis

1. Introduction

Remanufacturing was defined as a process of returning the used product to its original performance. And, it is required that performance specification of the remanufactured product should be equivalent to or even better than that of the new one. Remanufacturing engineering generally refers to the related techniques or engineering activities to remanufacture the waste products, which regards product life cycle theory as instructions and performance upgrading

as goals, with rules of energy-saving environment conservation-good quality-high efficiency by using advanced processing techniques [1]. It can bring great economic and social benefits on sources and environment to the world and has become an important way for sustainable society development [1–3].

Figure 1 shows the main procedures of used equipment remanufacturing process, which generally involves many steps such as disassembling, cleaning, detecting and assessing of the used components, remanufacturing, examining and reassembling of the remanufactured equipment. It also reveals that remanufacturing is supported by a series of relevant techniques during the whole process.

The remanufacturing forming procedure is of great importance to the quality of the remanufactured parts, which is also an obvious characteristic to distinguish remanufacturing production from manufacturing. As an advanced remanufacturing technology, laser remanufacturing can restore geometrical size and upgrade performance of the worn components with high productivity and little distortion, using laser cladding, laser welding, laser sintering or other laser-related processing methods [4, 5]. It has shown great benefits to the society for its successful applications over the last decade. More and more institutes, enterprises and industry sectors show great attentions to laser remanufacturing.

However, there are still some challenges for application of laser remanufacturing, especially residual stress-related problems such as brittle fracture, fatigue failure, stress corrosion cracking and buckling deformation [6]. As a research focus in recent years, residual stress has been experimentally measured by various damage detection methods such as hole drilling and indentation strain, as well as several non-destructive detection methods such as ultrasonic, X-ray diffraction and neutron diffraction methods. However, the experimental data are limited to thoroughly characterize the region distribution of residual stress. Hence, simulation method based on finite element model (FEM) is necessary to estimate the 3D residual stress field of the laser-remanufactured pieces. In this chapter, it introduces some researches on residual stress of laser remanufacturing metal pieces with cases of high-strength aluminium alloy, cast iron and high-strength steel, respectively.

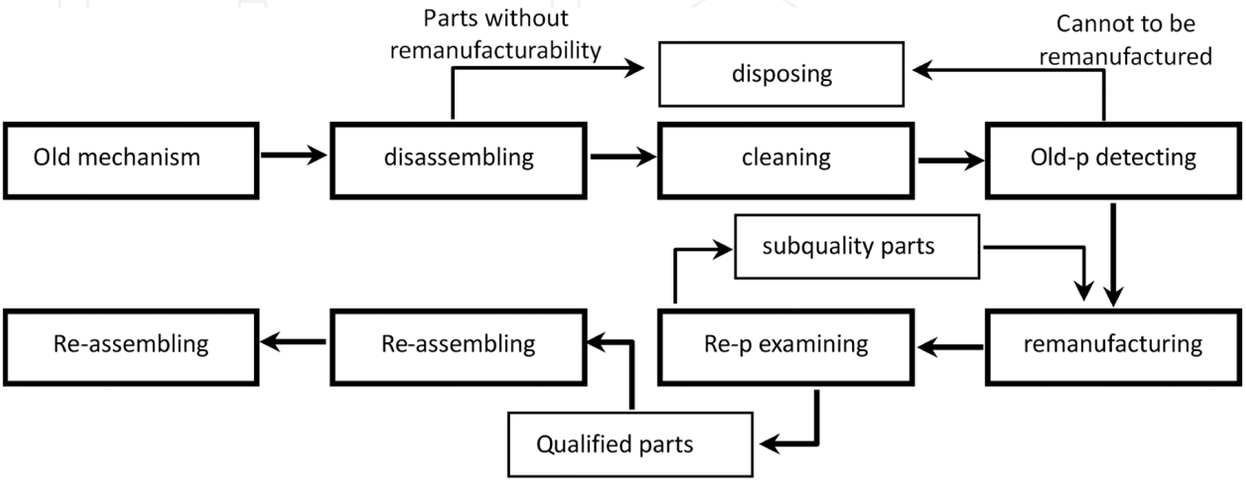

Figure 1. General procedures of mechanism remanufacturing.

2. Residual stress analysis of high-strength aluminium alloy pieces remanufactured by laser welding

Solidification cracking and stress corrosion cracking frequently occur in high-strength aluminium alloys, on the account of their relatively large linear expansion coefficients and high stress corrosion cracking susceptibility [7, 8]. Narrow gap laser welding (NGLW) is considered as one of the most effective ways to repair the cracks, for its lower heat input, less repairing deformation and better repairing quality, comparing with the conventional electric arc or plasma arc welding method [9–12]. However, residual stress of NGLW is also a vital factor for repairing quality of cracks and has been one of the research focuses of NGLW [13–15]. The aim of this work is to present distributions and evolution of residual stress during multipass NGLW processing.

2.1. Experimental procedure

The base material sample in this case was 7A52 aluminium alloy plates with dimensions of $50 \times 50 \times 20$ mm^3, and the filler wire was ER 5356 feed wire. A parallel I-type groove was applied, with gap width 3 mm and groove depth 18 mm, as shown in **Figure 2a**.

The six-pass NGLW was conducted by a 4 kW IPG fibre laser system with welding parameters: laser power 3.20 kW, welding speed 0.48 m/min and wire feed speed 2.15 m/min. A K-type thermocouple was used to detect temperatures during the six-pass NGLW processing, which was located in the heat-affected zone (HAZ) about 5 mm from the groove sidewall and 9 mm from the plate top surface.

2.2. Numerical simulation procedure

MSC.Marc 2016.0.0 software was exploited to simulate the six-pass NGLW processing without regard to the molten pool flow and droplet transfer behaviour. One-half of the symmetric geometric model was adopted as shown in **Figure 2b**. The values of material thermo-physical

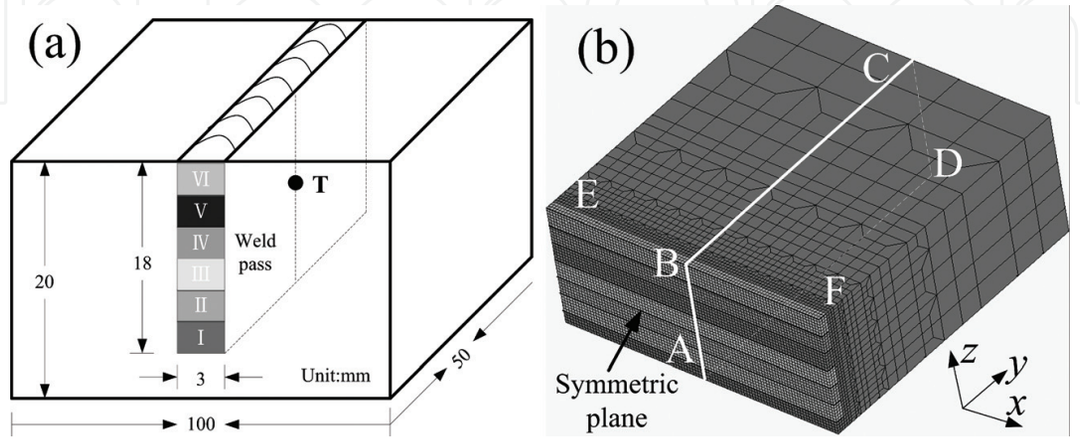

Figure 2. Sketch of the geometric model: (a) narrow gap groove and (b) mesh generation.

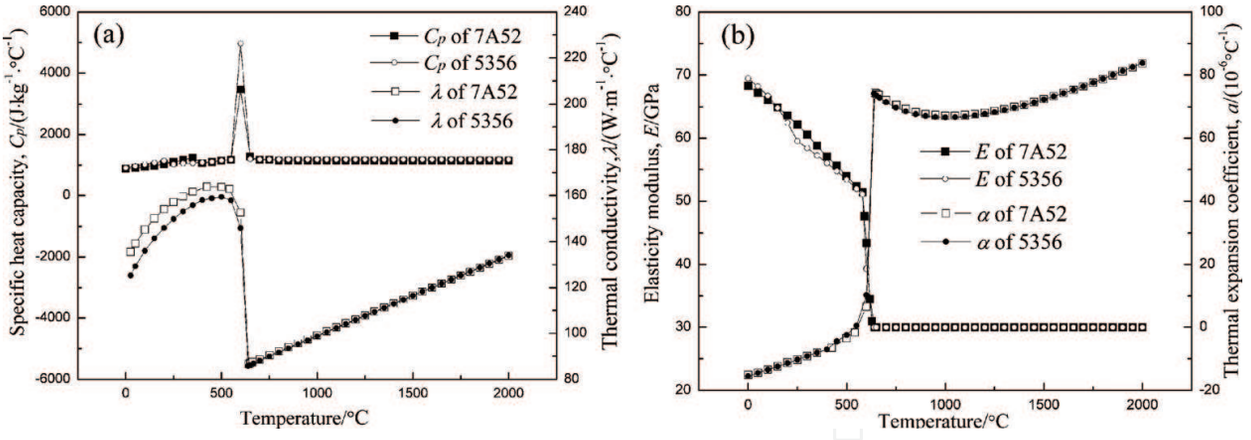

Figure 3. Thermo-physical values of 7A52 and 5356 aluminium alloys: (a) specific heat and thermal conductivity and (b) elasticity modulus and thermal expansion coefficient.

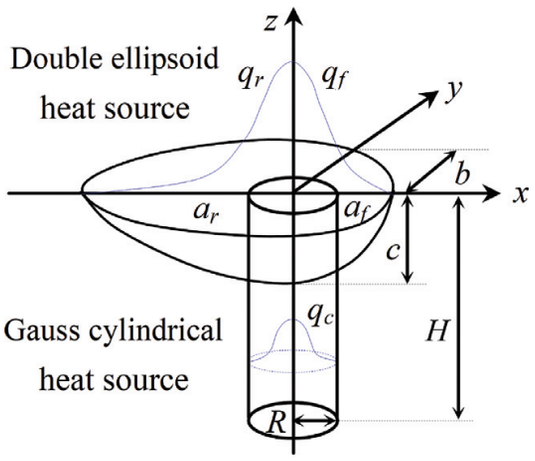

Figure 4. Sketch of the hybrid heat source model for NGLW.

property such as thermal conductivity thermal expansion coefficient and specific heat were estimated by the thermodynamic software JMatPro as given in **Figure 3**.

2.2.1. Heat source model

In order to more accurately describe the combined thermal effects of molten drop and laser irradiation on the base metal, a hybrid heat source model was adopted by combining double-ellipsoid heat source and Gauss cylindrical heat source, as shown in **Figure 4**.

The heat flux distribution in front half part (q_f) and latter half part (q_r) of the double ellipsoid could be, respectively, described as follows:

$$q_f(x,y,z) = \frac{6\sqrt{3}Q_1 f_f}{a_f bc\pi\sqrt{\pi}} \exp\left\{-3\left[\frac{(x-v_w t)^2}{a_f^2} + \frac{y^2}{b^2} + \frac{z^2}{c^2}\right]\right\} \tag{1}$$

$$q_r(x,y,z) = \frac{6\sqrt{3}Q_1 f_r}{a_r bc\pi\sqrt{\pi}} \exp\left\{-3\left[\frac{(x-v_w t)^2}{a_r^2} + \frac{y^2}{b^2} + \frac{z^2}{c^2}\right]\right\} \tag{2}$$

Parameter	a_f	a_r	f_f	f_r	b	c	R	H	β
Values	1.5 mm	4.0 mm	0.55	1.45	1.5 mm	2.5 mm	0.4 mm	4.0 mm	0.15

Table 1. The values of heat source parameters.

where a_f, a_r, b and c are the geometric parameters, v_w and t are the welding velocity and time and f_f and f_r are the distribution coefficient of heat flux determined by a_f and a_r.

The heat flux values (q_c) in Gauss cylindrical are characterized by Gaussian distribution in the radial direction and exponential decay along the depth, expressed as follows:

$$q_c(r,h) = \frac{6Q_2}{2\pi HR^2 + \beta\pi RH^2} \exp\left[\frac{-3r^2}{R^2}\right]\left[\frac{\beta h + R}{R}\right] \tag{3}$$

where R and H are the effective radius and height of Gauss cylindrical, respectively, and β is the energy attenuation coefficient.

Here, the adopted values of heat source parameters are given in **Table 1** on the basis of previous optimization by experimental observations to molten pool, measurements of joint on its cross section and comparisons between the simulated and experimental results.

2.2.2. Governing equations

The heat transfer phenomena in NGLW process is governed by the three-dimensional heat conduction equation for unsteady state:

$$\rho C_P \frac{\partial T}{\partial t} = \frac{\partial}{\partial x}\left(\lambda \frac{\partial T}{\partial x}\right) + \frac{\partial}{\partial y}\left(\lambda \frac{\partial T}{\partial y}\right) + \frac{\partial}{\partial z}\left(\lambda \frac{\partial T}{\partial z}\right) + Q_i + \Delta H \tag{4}$$

where ρ, λ and C_P are the density, thermal conductivity and specific heat, T is the temperature, Q_i is the internal heat source intensity and ΔH is the latent heat of fusion and crystallization. In this case, equivalent specific heat method was used to deal with ΔH, assuming that values of C_P had abrupt changes between the solidus and liquidus temperatures.

2.2.3. Boundary conditions

The symmetrical plane was assumed as adiabatic condition, while on other planes, heat transfer from metal substrate to atmosphere or backing plate occurred by means of thermal convection and radiation, and the thermal boundary condition can be defined as

$$-\lambda \frac{\partial T}{\partial n} = h_c(T - T_0) + \sigma\varepsilon\left(T^4 - T_0^4\right) \tag{5}$$

where λ is the thermal conductivity, T_0 is the atmosphere temperature, h_c is the convective heat transfer coefficient, σ is the Stephan-Boltzmann constant and ε is the emissivity.

As for the mechanical boundary conditions, the y-direction displacement of all nodes was fixed on the symmetrical plane to keep the balance of joint, while the nodes on the bottom plane and side edge were fixed in z direction to prevent rotational movement.

2.3. Result and discussions

2.3.1. Validation of the model

Figure 5 shows the comparison of calculated and measured temperature curves from the third pass during NGLW processing, which presents good agreement between them. The peak temperature of the calculated curve was 308.2°C, which was close to the measured 301.5°C. And the heating or cooling rates of the measured curve are slightly lower due to thermal inertia of thermocouple.

2.3.2. Evolution of transient stress field

Figure 6 shows the evolution of calculated transverse stress σ_y distribution in the middle of the first, third and fifth pass during NGLW processing. There is almost no stress existing in molten pool for melting of metal substrate. However, stress of its vicinity appears as compressive stress as a result of thermal expansion effect, which in turn leads to a tensile transverse stress at its distant zone. By comparing absolute value of the transverse stress and its concentration region in different weld passes, the existence of stress accumulation phenomenon can be confirmed during the multipass NGLW process.

2.3.3. Residual stress analysis

Figure 7 shows the 3D distributions of the numerically predicted transverse residual stress, longitudinal residual stress, vertical residual stress and von Mises equivalent residual stress in the joint. The concentration region of high residual stress is predominately presented in the weld zone or HAZ near the fusion line, where the latter part has higher values of von Mises equivalent stress than the front part for the gradual accumulations of distortion and stress, as shown in **Figure 7d**.

The residual stress distributions along the weld centre line EF and its vertical line BC, as marked in **Figure 1b**, are shown in **Figure 8**. Along the centre line of weld, both the transverse and longitudinal residual stresses show stable tensile stress characteristics with average values of 45.5 and 141.4 MPa, without regard to its unstable front and latter part. During the welding, rapid fusion and solidification appear along welding direction, accompanied by unbalanced

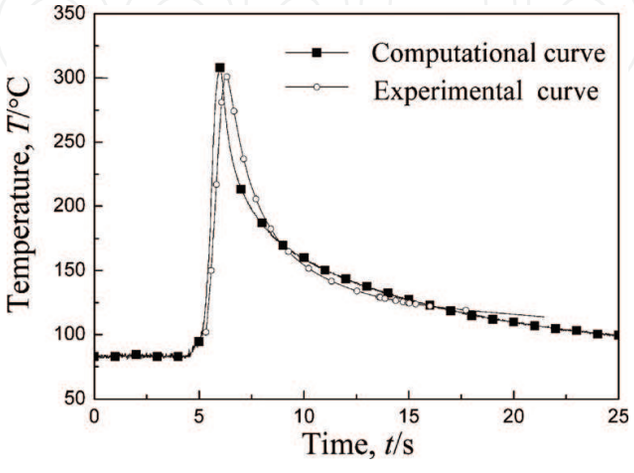

Figure 5. Calculated and measured temperature curves from the third pass.

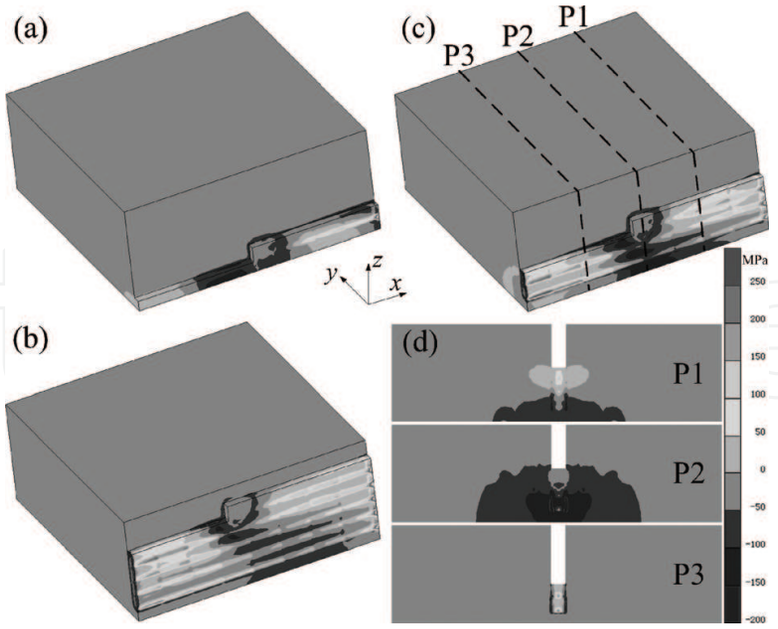

Figure 6. Distribution of transverse stress during the (a) first pass, (b) fifth pass, (c) and (d) third pass NGLW.

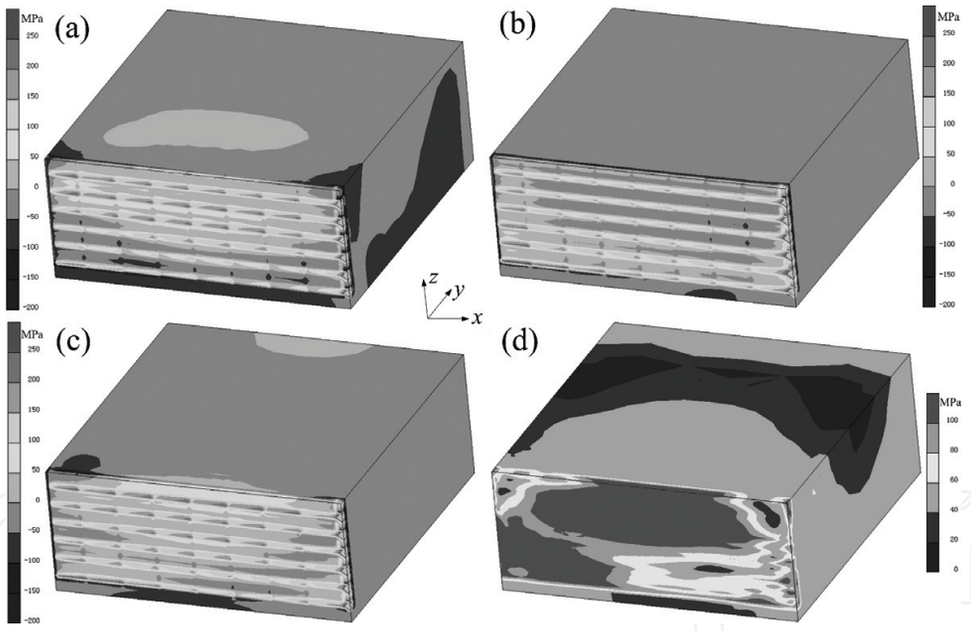

Figure 7. 3D residual stress distributions: (a) transverse residual stress σ_y, (b) longitudinal residual stress σ_x, (c) vertical residual stress σ_z and (d) von Mises equivalent stress.

expansion and shrinkage behaviours, resulting in higher longitudinal residual stress than the transverse residual stress. Nevertheless, the distribution of residual stress in its vertical direction is more complicated, as presented in **Figure 8b**. With increase of distance from the weld centre, values of transverse and longitudinal residual stress rapidly decline at the fusion line, and then the longitudinal residual stress decreases gradually until it turns into compressive residual stress from tensile stress, while the transverse residual stress begins to increase and then descends again, maintaining tensile residual stress all through.

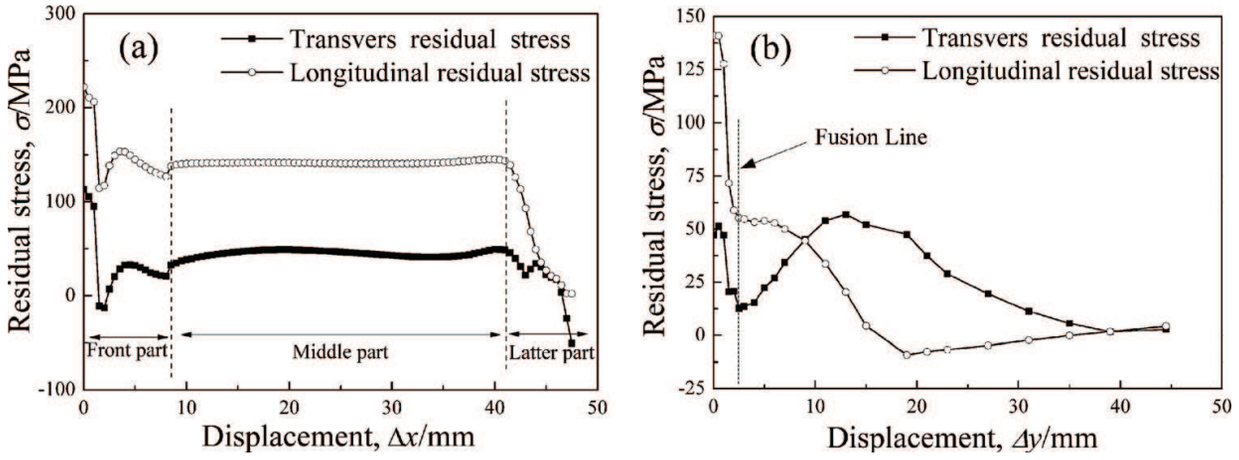

Figure 8. Residual stress distributions along (a) line EF and (b) line BC marked in **Figure 1b**.

3. Residual stress analysis of cast iron pieces remanufactured by laser cladding

QT 500 nodular casts iron as an industrial basic material is widely used in ship engines, crankshafts and machine tools [16–18]. As for laser cladding remanufacturing the cast iron pieces, due to the high carbon content, brittle phases are easily generated near the interface between the clad and substrate which causes residual stress during remanufacturing process. Therefore, study on residual stress and its control measures is vital to successful remanufacturing of cast iron components [19–21]. Two common laser pass-forming methods, parallel stacking forming and cross stacking forming, are chosen for the laser cladding process, as shown in **Figure 9**. A kind of Ni-Cu alloy power with element content of 0.03 wt.%C, 2.0 wt.%Si, 1.1wt.% B, 0.5wt.%Fe and 20.0 wt.%Cu and the balance Ni was selected as the cladding material, whose particle size scale was 20–106 μm.

3.1. Numerical simulation procedures

Thermal stress after cast iron laser cladding mainly comes from shrinkage of the clad layers during cooling process. Larger expansion coefficient difference between the substrate and the clad always caused larger residual stress after processing, which is usually a direct reason to the layer cracking. The cast iron parts are often large-scale castings, which can be considered as a fully constrained state around the forming layer.

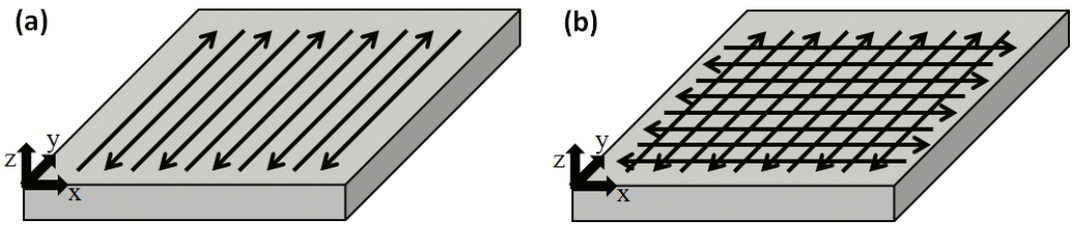

Figure 9. Sketch of the laser passes: (a) parallel stacking and (b) cross stacking.

Double-ellipsoid heat source model and Gauss body heat source model are often used to simulate the welding process, but the process of laser cladding is different with welding process; these heat source models are not suitable for simulating the cladding. Coupling of uniform body heat source (the energy density is same in different points of the heat source) and Gauss surface heat source was adopted in this experiment simulation process. The simulation uses ANSYS finite element software. Firstly, the stress evolution process under parallel stacking forming and cross stacking forming passes was simulated. Considering the actual remanufacturing process, the model is under one side constraint or fully constrained state. **Figure 10** is the temperature distribution at 2 and 5 s after multilayer laser cladding process, and **Figure 11** shows the temperature cycle curve of the fusion zone and the heat-affected zone. It can be seen that the clad layer and the heat-affected zone undergo repeated thermal cycles, which easily results in stress concentration.

Figure 12 shows the nephogram of the longitudinal stress, the deformation and macroscopic stress state in remanufacturing process. Ends of the sample in *x* direction are restrained. It can be seen that the stress is mainly concentrated around the constraint parts and the layers. **Figure 13** is the curve of the longitudinal stress of a node in the layer and a node in the substrate, and the node's location can be seen in **Figure 12**. The layer mainly presents the tensile stress state, while the substrate is mainly in the state of compressive stress. For the actual remanufacturing process, the constraints should be avoided or removed as far as possible.

3.2. Experimental procedure

In order to obtain the residual stress distribution in the surface and interior of the clad layer, *X*-ray diffraction method was used for measuring the accumulation of residual stress in the clad layer. The electrolytic etching method was used to peel clad layer from the top surface to the internal layer, and the thickness of the peeling layer is 60 μm. Residual stress parallel or vertical to the cladding line was tested, respectively, at a certain point, and the schematic diagram of the test is shown in **Figure 14**.

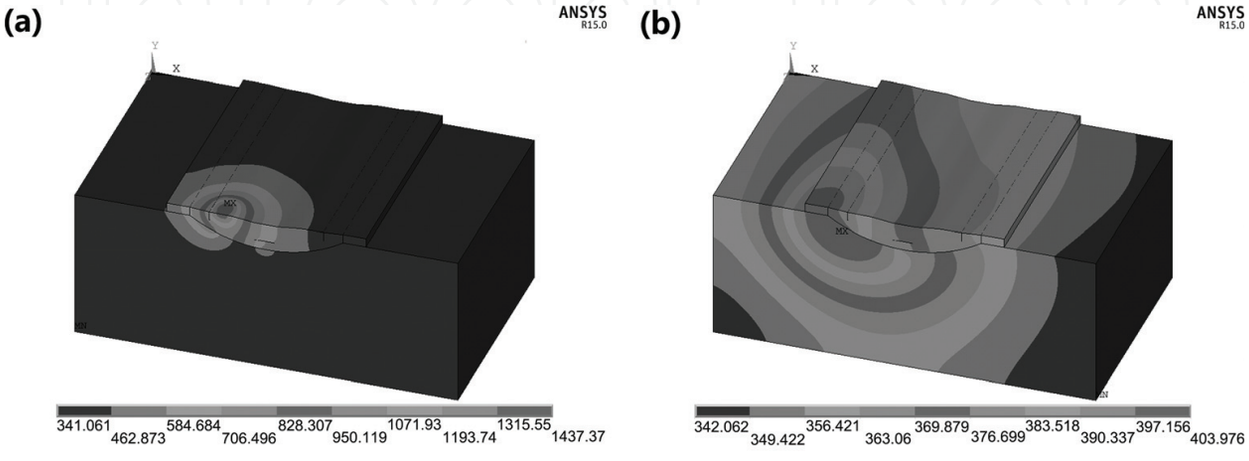

Figure 10. Temperature distribution at (a) 2 and (b) 5 s.

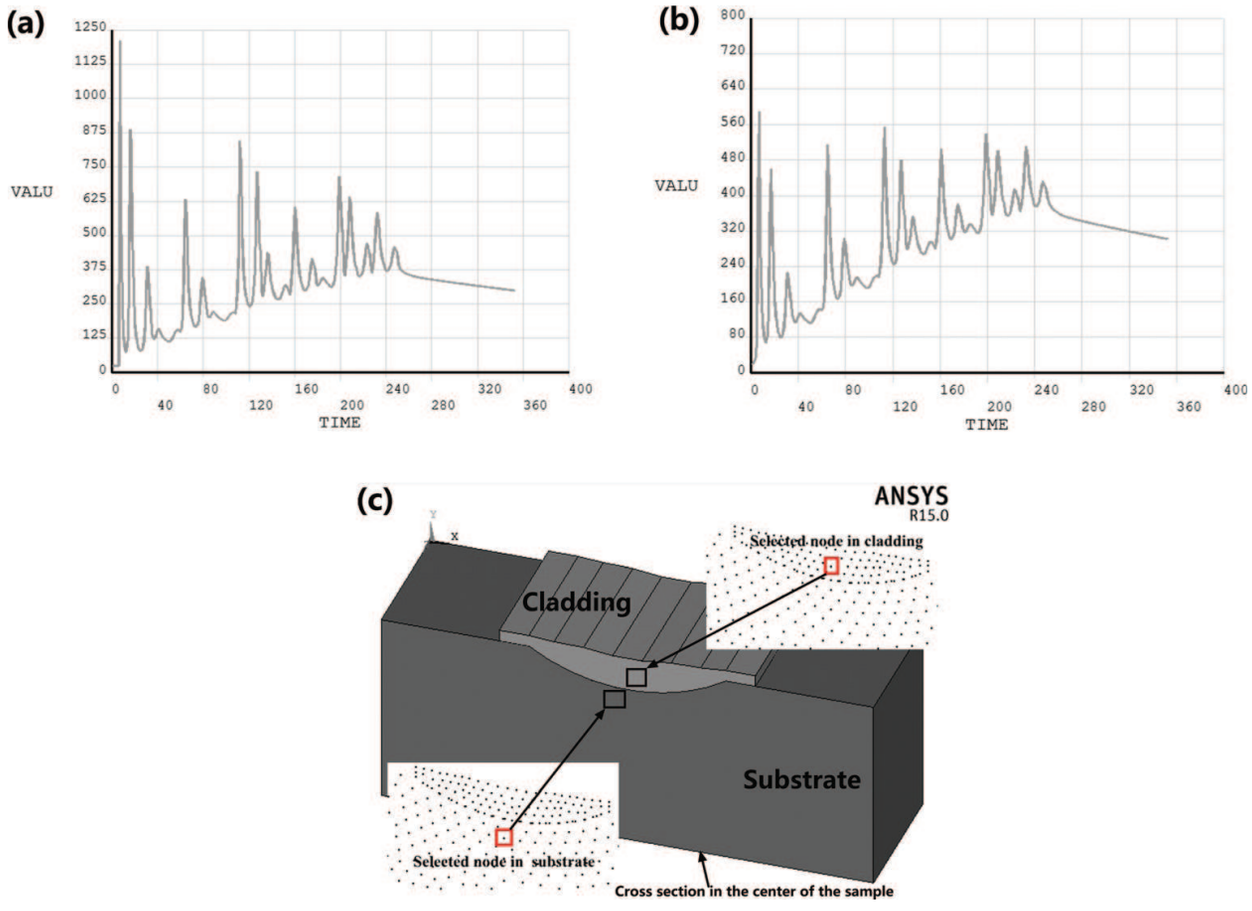

Figure 11. Temperature distribution of different zones: (a) the fusion zone and (b) the HAZ (c) location of the selected nodes.

3.3. Results and discussions

Figure 15 shows residual stress distribution in different scanning passes in the clad layer. It can be found that residual stress increases slowly from the surface to inside of the layers formed by cross stacking method. The state of stress is tensile stress with the highest value +300 MPa. The residual stress of the clad layer formed by the parallel path is fluctuated from the surface to the interior, and the fitting curve shows a downward trend. The residual stress at the top of the clad layer reaches the highest tensile stress, reaching +380 MPa, and the lowest residual stress is 50 MPa inside the clad layer. It can be seen that the residual stress of the cross path cladding is smaller than that of the parallel path in the range of 340 μm depth from the surface, and beyond this range, residual stress changes in opposite direction. Residual stress distribution vertical to cladding line direction of the cladding is shown in **Figure 15b**. It can be found that residual stress from the surface to the interior in the clad layer in two kinds of forming methods is increased, but the residual stress in the layers formed in cross path is smaller than that of parallel path at different depths. It can be seen that the cross path forming is beneficial to reduce the thermal stress of the clad layer in the vertical direction.

The thermal cycle curve of the cross stacking forming shows irregular and overlapping effect, and the interval between two adjacent temperature peaks is relatively large. Therefore, there is

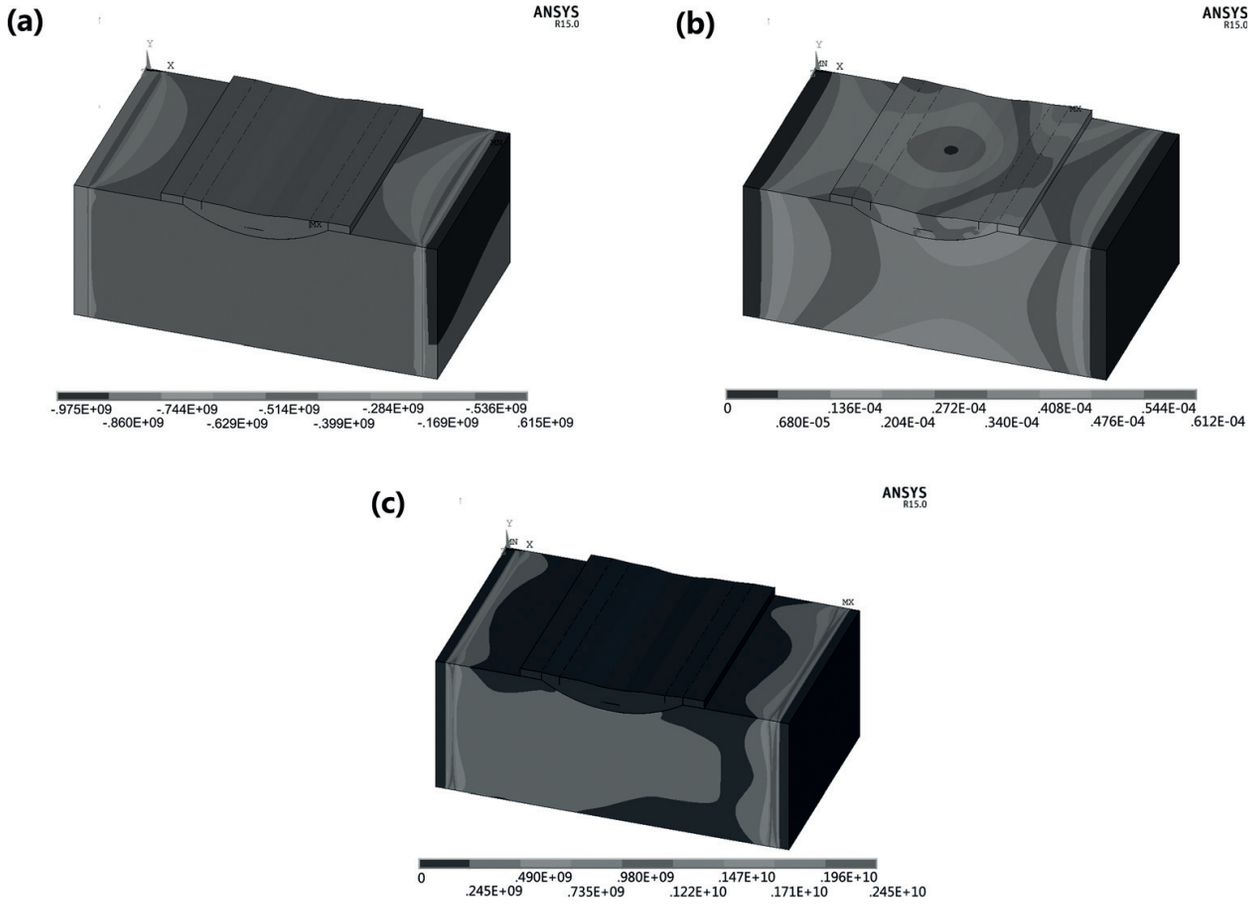

Figure 12. Nephogram of stress and deformation: (a) longitudinal stress, (b) deformation and (c) macroscopic stress.

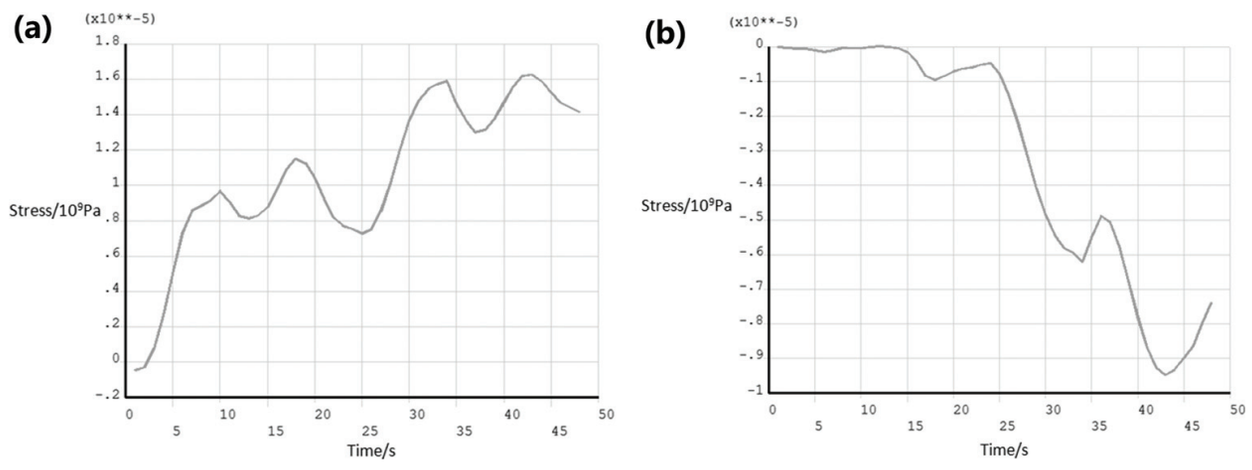

Figure 13. Stress curves of the (a) selected node in the layer and (b) selected node in the substrate.

no apparent periodic heat accumulation in the clad layer, and the heat dispersion effect is obvious. Therefore, characteristics of the temperature field with relatively small temperature gradient caused smaller shrinkage difference of the clad layer, and the thermal stress in the clad layer decreased. The thermal cycling curves of parallel path forming show apparent

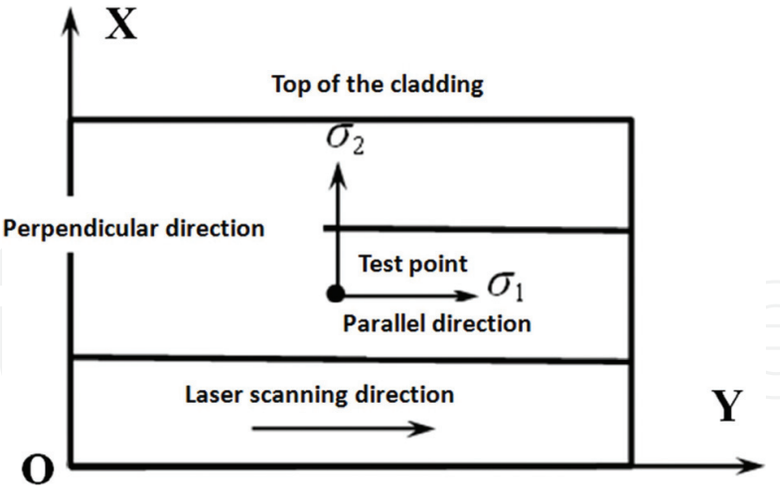

Figure 14. Schematic diagram of residual stress tests.

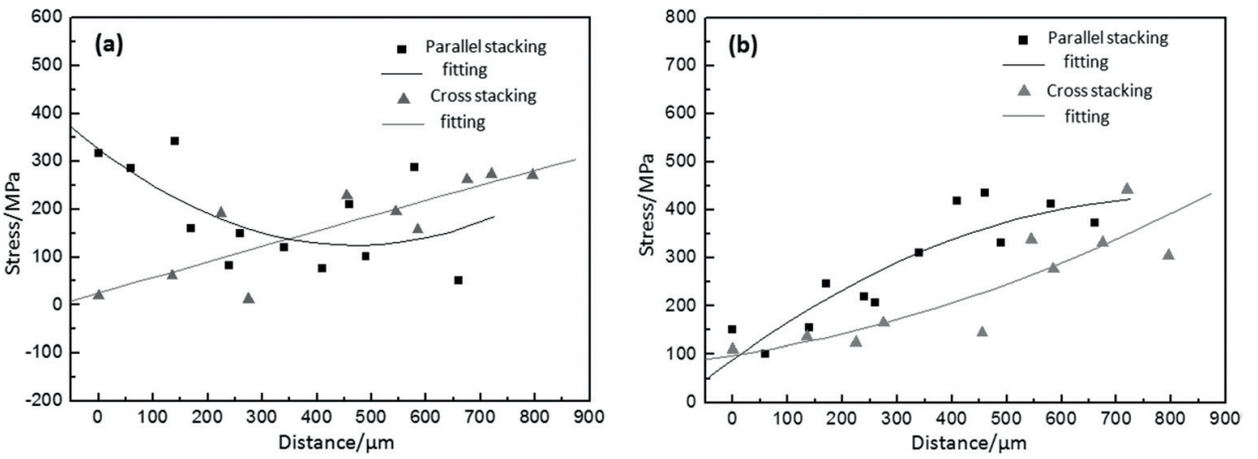

Figure 15. Residual stress in different scanning passes: (a) parallel and (b) vertical to cladding line.

periodic thermal cumulative effect and heat accumulation of the clad layers, then large temperature gradient exists between high-temperature area of molten pool and the ambient clad layer and the shrinkage deformation and the stress of layers increases. Therefore, the cross path forming is beneficial to the thermal stress control of the clad layer.

Figure 16 shows residual stress distribution in the clad layer with different laser powers. It shows that the residual stress differs obviously in the parallel direction and vertical direction when the power increased from 800 to 1200 W. The residual stress decreases apparently in the layers parallel to cladding direction when depth increases. The residual stress in the surface reaches 120 MPa. In depth of 60 μm layer, the tensile stress begins to change into the compressive stress, and in depth of 600 μm, the residual stress reached −300 MPa in the clad layer. In contrast, stress decreases slowly when the power is 800 W.

In the vertical direction of the cladding line, with the increase of layer depth, residual tensile stress of clad layer increases from the surface to the interior when the power reaches 1200 W. The curve slope becomes larger, which means that the stress increases persistently with the

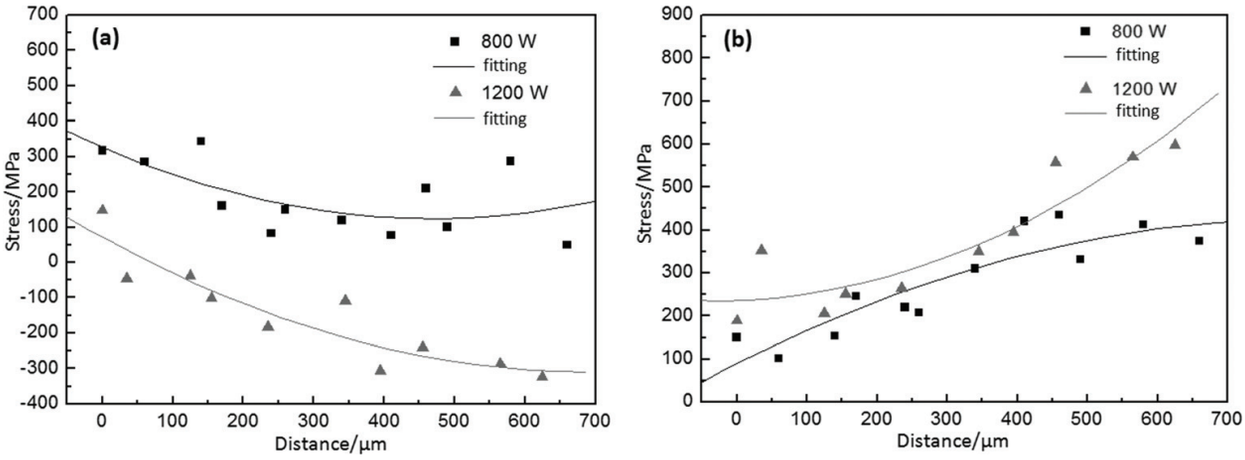

Figure 16. Residual stress curves in different laser powers: (a) parallel and (b) vertical to cladding line.

increase of the depth. At the depth of 600 μm, the residual tensile stress of the clad layer reaches 600 MPa, approaching the tensile strength of the clad layer, and the cracking tendency of the deposited clad layer increases. Therefore, the stress distribution characteristics of the clad layer under 1200 W are poor, and the cracks may exist in the clad layer. This also verifies that the low-power cladding process has good quality control effect on the remanufacturing of cast iron castings.

According to the analysis of temperature field at the laser power of 800 and 1200 W, with the increase of laser power, the peak temperature of the thermal cycle curve increases significantly, and the temperature gradient of molten pool and gradient around the area increases. Reduction of cooling time causes cooling velocity to increase rapidly and results in the increasing of elastic-plastic deformation of cladding under residual stress. After solidification, the residual stress distribution along different directions is shown in **Figure 16**.

To sum up, temperature field of laser cladding during cladding process has an important influence on the residual stress of the laser cladding. The results of the simulation and the actual test show that for the remanufacturing process of cast iron, it can be to helpful to reduce the overall residual stress by using cross path method, and lower heat input causes lower residual stress. These two methods result in the homogenization of the expansion and contraction of the layers during cladding process; therefore, the deformation is smaller, and the residual stress is relatively low. Therefore, from the point of view of controlling the residual stress of the clad layer, using low power and cross path method are used to control the residual stress of the clad layer.

4. Residual stress analysis of high-strength steel pieces remanufactured by laser cladding

During the complex thermal cycling of laser cladding, the high-strength steel, solid phase transition, such as eutectoid reaction, solid solution reaction, austenite transition and martensitic transition usually take place. Solid-state phase transition, which is accompanied by specific

volume change, transition plasticity and some other effects, will affect the stress field and final residual stress distribution.

The occurrence of solid-state phase transition may have a certain impact on laser cladding or other welding processes under certain conditions. In some cases, the effect is even dominant. Since transition-induced plasticity increases the martensitic transition temperature, the martensitic transition has a significant effect on distribution of residual stress [22]. Ohta [23] studied the effect of solid phase transition on the evolution of residual stress and analysed the influence of diffusion phase transition and non-diffusion phase transition on residual stress. Materials with low phase transition point will result in lower residual stresses; the effect of solid-state phase transition on mechanical properties, solid phase transition volume effect and solid-state phase transition plasticity is the main factors affecting the stress evolution [24].

For steel, it is a hotspot to consider the solid-state phase transition effect in the process of laser cladding thermal-machine simulation. However, the actual situation is complex and still has some work to be done [25]. Firstly, the coupling interaction is very complicated since the stress has a great effect on the phase transition temperature and phase transition kinetics, which in turn affects the evolution of stress. Secondly, the tempering effect accompanying the thermal cycling will affect the physical properties and phase transition properties of the material. Then, many work lacks systematic and reliable physical data, especially computer simulation, in which the systematic and reliability of the data is a very important factor. Moreover, the research results are mostly limited to the welding process [25, 26].

4.1. Numerical simulation procedure

The laser cladding is a processing with multi-parameter, complex nonlinearity and strong coupling and has a wide variety of scanning strategies; the scanning strategy is in direct relation to the thermal cycle of the laser cladding process, which has great influence on the stress, strain and microstructure of the remanufacturing part. Based on a few simplification and assumptions, computer simulation can try all kinds of process parameters and provides the temperature and stress data of remanufacturing part at any point and any time for the analysis of stress, microstructure and properties evolution.

Austenite is set as the initial phase in the solidification process. As temperature decreases, the martensitic phase transition starts at Ms (the martensite starting temperature) and finishes at Mf (the martensite finishing temperature). The volume fraction of martensite phase (f_M) can be shown as [27]

$$f_M = 1 - f_{\gamma 0}\Phi(T) \tag{6}$$

$$\Phi(T) = \left\{ \begin{array}{ll} 1 & T \geq M_s \\ \exp(-\alpha(M_s - T)) & T < M_s \end{array} \right\} \tag{7}$$

where $f_{\gamma 0}$ is the initial austenitic volume percentage and $f_{\gamma 0}\Phi$(T) is the ratio of austenite at a specific temperatures α is the kinetics coefficient of phase change, and can be obtained by experiments.

Phase transition plasticity refers to the plastic strain of the material under the external load which is much less than yield strength. It mainly comes from the Greenwood-Johnson mechanism and the Magee mechanism. According to the classic work of Inoue, Leblond and Fisher, considering that during the laser cladding processing the longitudinal residual stress value is close to that of yield strength, the expression of the stress increment should be revised to

$$\Delta\varepsilon^{Trp} = -\frac{2\Delta\varepsilon_{\alpha\gamma}}{\sigma_{\gamma}^{y}\left(\varepsilon_{\gamma}^{eff}\right)}\ln\left(f_M\right)\Delta f_M \cdot h\left(\frac{\sigma^{eq}}{\sigma^{y}}\right)\cdot S_{ij} \tag{8}$$

where $\Delta\varepsilon_{\alpha\gamma}$ is the strain difference between austenite and martensite considering the volume effects of phase transition, $\sigma_{\gamma}^{y}\left(\varepsilon_{\gamma}^{eff}\right)$ is the yield strength of high-temperature phase (taking into account the hardening effect), S_{ij} is the deviatoric stress tensor and f_M is the volume fraction of martensite.

The expression above is complex, and in practice the related parameters are difficult to obtain. A simplified equation is put forward [25]:

$$\Delta\varepsilon^{Trp} = 3k\left(1 - f_M\right)\Delta f_M \cdot S_{ij} \tag{9}$$

where k is easily obtained by experiments.

It is assumed that the initial and final austenitic ratio is f'γ_0 and 100% when the temperature rises to Ac_1 and Ac_3, respectively; the percentage of austenite phase increases linearly as temperature rises. Once the temperature is lower than Ms, austenite will partially or totally transform into martensite during the subsequent cooling period. The martensite tempering and formation of interdendritic eutectic phase during solidification are neglected.

In this work, under the condition of single-pass deposition, three kinds of situations are analysed in comparison: the two are phase transition (one considering stress influence) and the other one without phase transition. We obtained the following characteristics by experiments: expansion coefficient of martensite state is about 18.75×10^{-6}/°C (room temperature) and rises up to ~19×10^{-6}°C (at above 600°C); Ms = 160°C, Ac1 = 600°C and Ac3 = 900°C; the volumetric change strain is 0.0067352; kinetic coefficient of the phase transition during the cooling period is ~0.02347; and parameter of transition plasticity is 1.165×10^{-4}. Molten pool convection is simulated indirectly by elevated thermal conductivity coefficient (twice as large as that of room temperature) and the double-ellipsoid heat source. Latent heat (283 J/g) is taken into consideration when melting and solidification take place. The emissivity (ε) is defined to be 0.5, and the convection coefficient (h_c) is 30 W/m^2 K. Initial temperature is set at 25°C (room temperature). Finally, the deposition process is regarded as quasi-steady process, and the materials are assumed isotropic [25].

4.2. Experimental measuring procedure

In the same piece of substrate, under the same experimental conditions, technological parameters and using different material powders (with phase transition and without phase transition,

	C	Cr	Ni	Mo	Mn	Nb	Si	B	Cu	Fe
1	0.13	12.8	4.7	—	—	—	1.0	1.4	—	Bal
2	0.03	—	Bal	—	—	—	2	1.1	20	0.5
3	0.03	17.5	14	2.3	2.0	—	1.0	—	—	Bal
4	0.1	15	10	—	—	—	1.0	1.0	—	Bal
5	0.03	13.8	4.5	1.0	0.7	0.35	0.5	—	—	Bal
6	0.12	15.4	4.2	1.4	0.6	—	1.4	0.8	—	Bal
7	0.05	—	Bal	—	—	—	2.7	1.8	—	0.4

Table 2. The ingredients of the used laser cladding alloying powders.

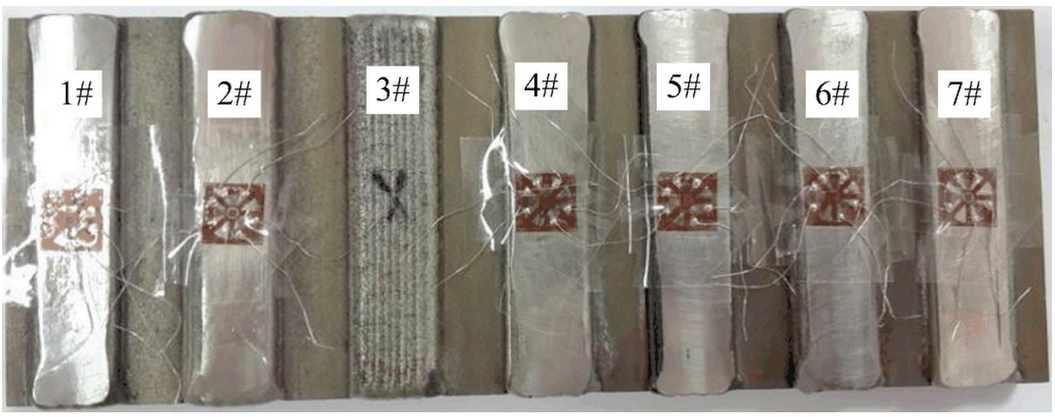

Figure 17. The laser cladding samples of different alloying powders.

	M_s (°C)	Y_s (MPa)	σ_1 (MPa)	σ_2 (MPa)	σ_e (MPa)
1	250	1280	163.44	−32.06	181.60
2	None	—	88.86	−8.11	73.26
3	Below RT	—	—	—	—
4	Below RT	720	430.07	111.04	386.69
5	158	920	−196.91	−307.47	269.75
6	190	1150	−67.52	−169.83	148.11
7	None	530	349.26	187.61	302.75

Table 3. The result of the residual stress (RT, room temperature).

respectively) as shown in **Table 2**, the hole drilling method is used for measurement of residual stress of different powders in one position.

In this case, FV520B is martensitic precipitation-hardening steel with excellent strength and good welding performance and is used as the substrate. These samples (**Figure 17**) are clad layers of different materials, and the scanning strategy is arch deposition (as shown in **Table 2**).

The technology parameters of the laser cladding process are as follows: energy power is 1.8 kW; scanning rate is 8 mm/s; width of a single track is 3 mm; and lapping rate is 0.5.

The residual stress results are shown in **Table 3**; it can be seen that:

1. For samples with solid-state phase transition, the first principal stress values are both low; #5 and #6 samples show compressive stress, and #1 sample is in tension stress state, whose value is at about 12.7% of the yield stress in the room temperature.
2. For most samples with no solid-state phase transition, the first principal stress of tension stress state and the stress value are high.
3. For materials with solid-state phase transition, the higher solid-state phase transition temperature means higher residual stress obtained.

4.3. Result and discussions

Figure 18 shows the residual stress distribution under the condition of single-pass deposition. Firstly, the stress distribution is nearly the same in the area away from the cladding bead. For the case with phase transition considered (**Figure 18b**), it is obvious that the stresses are lower in the clad bead as well as the adjacent region. Moreover, the interface between the cladding and substrate shows a lower stress level than that of the clad layer and substrate. The maximum tensile stress is observed at about a few millimetres from the surface of the clad layer. Nonetheless, when the phase transition is ignored (**Figure 18a**), the residual stresses in the cladding bead increase obviously, which are near the yield strength; the maximum tensile stress is found in the interface between the substrate and the clad layer. When phase transition is taken into account, the cases with and without considering the stress effect on phase transition temperature (**Figure 18c** and **d**, respectively) show a similar residual stress level and distribution [25].

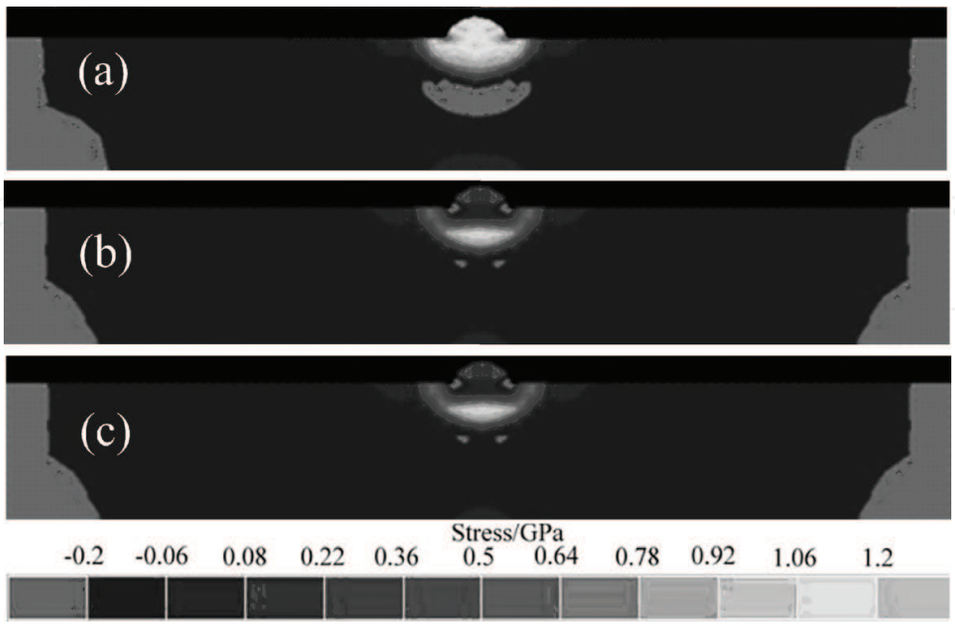

Figure 18. Stress distribution of single-layer laser clad sample: (a) ignore phase transition (b) considering phase transition, and ignore the stress effect on phase transition temperature (c) considering both phase transition and stress effect on phase transition temperature.

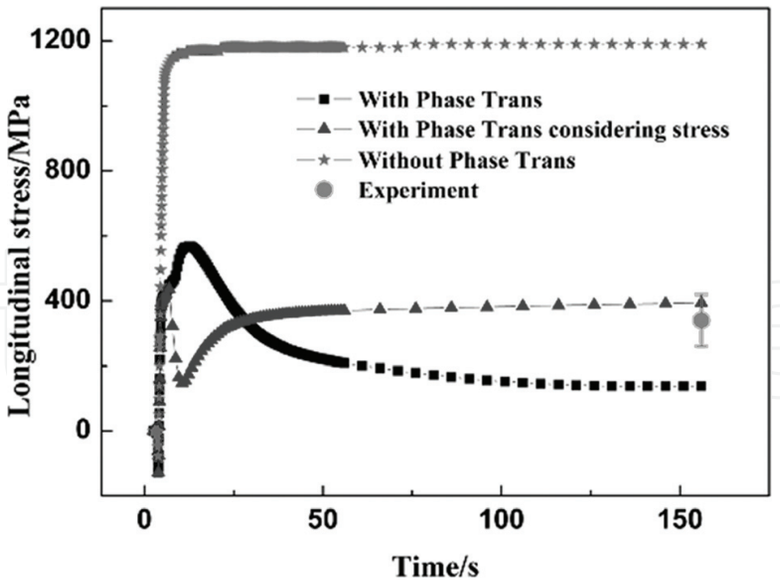

Figure 19. Longitudinal stress of a single-pass laser clad from calculation and experiment determination.

Figure 19 shows longitudinal residual stress evolution (*z* direction, along the laser travel) of the midpoint in a clad layer. The simulation results are in contrast to the results obtained by experimental determination. When the phase transition is ignored, the residual longitudinal stress is close to the yield strength (around 1200 MPa). When considering the phase transition, as the temperature decreases, the maximum longitudinal stress is around 600 MPa and finally stabilized at around 200 MPa. When the stress influence on phase transition temperature is considered, the residual longitudinal stress is closer to the experimental results (394 MPa) than the other two cases. Generally speaking, phase transition has an obvious effect on the residual stresses, making it a more accurate simulation result.

5. Conclusions

Laser remanufacturing is an advanced repairing method to restore the damaged parts based on laser processing, such as laser cladding and laser welding. To avoid obvious distortion and severe residual stress concentration, it is necessary to carry out residual stress analysis by numerical simulation and experimental methods. For high-strength aluminium alloy parts remanufactured by multipass NGLW process, welding passes have obvious effects on the distribution of residual stress, and its accumulation phenomenon would be exacerbated with the increase of welding passes. From the point of view of controlling the residual stress, low laser power and cross path forming strategies were suggested for their important influences on the residual stress in the laser clad layer of nodular cast iron pieces. For high-strength steel with solid-state phase transition remanufactured by laser cladding, the phase transition from austenite to martensite during the cooling process had a positive influence to reduce the magnitude of residual stresses, and a lower residual stress can be obtained using alloying powder materials with lower solid-state phase transition temperature.

Acknowledgements

The work was supported by the key programme of the National Key Research and Development of China (Grant No. 2016YFB1100205), NSFC programme (Grant No.51705532) and Beijing Science and Technology projects (Grant No. Z161100004916009, Z16110000 1516007).

Author details

Shi-yun Dong*, Chao-qun Song, Xiang-yi Feng, Yong-jian Li and Shi-xing Yan

*Address all correspondence to: syd422@sohu.com

National Key Laboratory for Remanufacturing, Beijing, China

References

[1] Xu BS. Theory and technology of equipment remanufacturing engineering. National Defense Industrial Press, Beijing, China; 2007

[2] Xu Bs, Dong sy, Zhu S, et al. Prospects and developing of remanufacture forming technology [J]. Journal of Mechanical Engineering. 2012;**48**(15):96-105. DOI: 10.3901/JME.2012.15.096

[3] Cunha JO, Konstantaras I, Melo RA, et al. On multi-item economic lot-sizing with remanufacturing and uncapacitated production. Applied Mathematical Modelling. 2017;**50**: 772-780. DOI: 10.1016/j.apm.2016.10.037

[4] Xu BS, Dong SY. Laser Remanufacturing Technology. Beijing, China: National Defense Industry Press; 2016

[5] Dong SY, Xu BS, Wang ZJ, et al. Laser remanufacturing technology and its applications. Lasers in Material Processing and Manufacturing III. 2007;**6825**:68251N. DOI: 10.1117/12.782335

[6] De A, DebRoy T. A perspective on residual stresses in welding. Science and Technology of Welding and Joining. 2011;**16**(3):204-208. DOI: 10.1179/136217111X12978476537783

[7] Hu B, Richardson IM. Mechanism and possible solution for transverse solidification cracking in laser welding of high strength aluminium alloys. Materials Science and Engineering: A. 2006;**429**(1):287-294. DOI: 10.1016/j.msea.2006.05.040

[8] Sheikhi M, Ghaini FM, Assadi H. Prediction of solidification cracking in pulsed laser welding of 2024 aluminum alloy. Acta Materialia. 2015;**82**:491-502. DOI: 10.1016/j.actamat.2014.09.002

[9] Guo W, Li L, Dong SY, et al. Comparison of microstructure and mechanical properties of ultra-narrow gap laser and gas-metal-arc welded S960 high strength steel. Optics and Lasers in Engineering. 2017;**91**:1-15. DOI: 10.1016/j.optlaseng.2016.11.011

[10] Dittrich D, Schedewy R, Brenner B, et al. Laser-multi-pass-narrow-gap-welding of hot crack sensitive thick aluminum plates. Physics Procedia. 2013;**41**:225-233. DOI: 10.1016/j.phpro.2013.03.073

[11] Zhang ZH, Dong SY, Wang YJ, et al. Microstructure characteristics of thick aluminum alloy plate joints welded by fiber laser. Materials & Design. 2015;**84**:173-177. DOI: 10.1016/j.matdes.2015.06.087

[12] Zhang ZH, Dong SY, Wang YJ, et al. Study on microstructures and mechanical properties of super narrow gap joints of thick and high strength aluminum alloy plates welded by fiber laser. The International Journal of Advanced Manufacturing Technology. 2016;**82**(1–4): 99-109. DOI: 10.1007/s00170-015-7334-5

[13] Guo W, Francis JA, Li L, et al. Residual stress distributions in laser and gas-metal-arc welded high-strength steel plates. Materials Science and Technology. 2016;**32**(14):1449-1461. DOI: 10.1080/02670836.2016.1175687

[14] Elmesalamy A, Francis JA, Li L. A comparison of residual stresses in multi pass narrow gap laser welds and gas-tungsten arc welds in AISI 316L stainless steel. International Journal of Pressure Vessels and Piping. 2014;**113**:49-59. DOI: 10.1016/j.ijpvp.2013.11.002

[15] Phaoniam R, Shinozaki K, Yamamoto M, et al. Solidification cracking susceptibility of modified 9Cr1Mo steel weld metal during hot-wire laser welding with a narrow gap groove. Welding in the World. 2014;**58**(4):469-476. DOI: 10.1007/s40194-014-0130-2

[16] Jeshvaghani RA, Harati E, Shamanian M. Effects of surface alloying on microstructure and wear behavior of ductile iron surface-modified with a nickel-based alloy using shielded metal arc welding. Materials and Design. 2011;**32**(3):1531-1536. DOI: 10.1016/j.matdes.2010.10.006

[17] Pouranvari M. On the weldability of grey cast iron using nickel based filler metal. Materials & Design. 2010;**31**(7):3253-3258. DOI: 10.1016/j.matdes.2010.02.034

[18] Cheng X, Hu SB, Song WL, et al. Improvement in corrosion resistance of a nodular cast iron surface modified by plasma beam treatment. Applied Surface Science. 2013;**286**(4): 334-343. DOI: 10.1016/j.apsusc.2013.09.083

[19] Abboud JH. Microstructure and erosion characteristic of nodular cast iron surface modified by tungsten inert gas. Materials & Design. 2012;**35**:677-684. DOI: 10.1016/j.matdes.2011.09.029

[20] Zhong ML, Liu WJ, Zhang HJ. Corrosion and wear resistance characteristics of NiCr coating by laser alloying with powder feeding on grey iron liner. Wear. 2006;**260**(11–12): 1349-1355. DOI: 10.1016/j.wear.2005.09.033

[21] Ghaini FM, Ebrahimnia M, Gholizade S. Characteristics of cracks in heat affected zone of ductile cast iron in powder welding process. Engineering Failure Analysis. 2011;**18**(1):47-51. DOI: 10.1016/j.engfailanal.2010.08.002

[22] Bhadeshia H. Phase transformations contributing to the properties of modern steels. Bulletin of the Polish Academy of Sciences Technical Sciences. 2010;**58**(2):255-265. DOI: 10.2478/v10175-010-0024-4

[23] Ohta A, Suzuki N, Maeda Y, et al. Fatigue strength improvement of lap welded joints by low transition temperature welding wire—Superior improvement with strength of steel. Welding in the World. 2003;**47**(3–4):38-43. DOI: 10.1533/weli.18.2.112.27124

[24] Hu LX, Dongpo W, Wenxian W, et al. Ultrasonic peening and low transition temperature electrodes used for improving the fatigue strength of welded joints. Welding in the World. 2004;**48**(3–4):34-39. DOI: 10.1007/BF03266425

[25] Fang JX, Dong SY, Wang YJ, et al. The effect of solid-state phase transition upon stress evolution in laser metal powder deposition. Materials & Design. 2015;**87**:807-814. DOI: 10.1016/j.matdes.2015.08.061

[26] Francis JA, Bhadeshia H, Withers PJ. Welding residual stresses in ferritic power plant steels. Materials Science and Technology. 2007;**23**(9):1009-1020. DOI: 10.1179/174328407X213116

[27] Koistinen DP, Marburger RE. A general equation prescribing the extent of the austenite-martensite transition in pure iron-carbon alloys and plain carbon steels. Acta Metallurgica. 1959;**7**(1):59-60. DOI: 10.1016/0001-6160(59)90170-1

IntechOpen